Research Article | Vol. 11, No. 4 / 1 April 2020 / Biomedical Optics Express 1901
Biomedical Optics EXPRESS

Determination of refractive index, size, and solid content of monodisperse polystyrene microsphere suspensions for the characterization of optical phantoms

PETER NAGLIČ,* YEVHEN ZELINSKYI, BOŠTJAN LIKAR, AND MIRAN BÜRMEN

University of Ljubljana, Faculty of Electrical Engineering, Laboratory of Imaging Technologies, Tržaška cesta 25, SI-1000, Ljubljana, Slovenia
peter.naglic@fe.uni-lj.si

Abstract: Monodisperse polystyrene microspheres are often utilized in optical phantoms since optical properties such as the scattering coefficient and the scattering phase function can be calculated using the Mie theory. However, the calculated values depend on the inherent physical parameters of the microspheres which include the size, refractive index, and solid content. These parameters are often provided only approximately or can be affected by long shelf times. We propose a simple method to obtain the values of these parameters by measuring the collimated transmission of polystyrene microsphere suspensions from which the wavelength-dependent scattering coefficient can be calculated using the Beer-Lambert law. Since a wavelength-dependent scattering coefficient of a single suspension is insufficient to uniquely derive the size, refractive index and solid content by the Mie theory, the crucial and novel step involves suspending the polystyrene microspheres in aqueous sucrose solutions with different sucrose concentrations that modulates the refractive index of the medium and yields several wavelength-dependent scattering coefficients. With the proposed method, we are able to obtain the refractive index within 0.2% in the wavelength range from 500 to 800 nm, the microsphere size to approximately 15 nm and solid content within 2% of their respective reference values.

© 2020 Optical Society of America under the terms of the OSA Open Access Publishing Agreement

1. Introduction

Optical phantoms are often utilized for calibration of optical systems [1] and validation of inverse models for estimation of optical properties [2]. While optical phantoms can come in liquid [3] or solid form [4], water-based suspensions of nearly monodisperse polystyrene microspheres are especially attractive since the optical properties, such as the scattering coefficient and scattering phase function, can be derived using the Mie theory [5]. Suspensions of polystyrene microspheres (SPMs) also come in standardized forms and exhibit significantly smaller batch-to-batch variations in comparison to some other liquid or solid phantoms. Furthermore, the optical properties of other phantoms have to be measured by a well-validated optical modality that is not readily available in every laboratory or institution [4]. These modalities can also introduce bias and uncertainty into the estimated values of optical properties.

Even though the optical properties of SPMs can be accurately derived from the Mie theory, the accuracy of calculated values still depends on the inherent physical properties of the microspheres. Among these properties is the size distribution of the microspheres, which is for commercially available SPMs usually modeled by a Gaussian distribution with supplier-provided mean and standard deviation of the diameter. In our experience, the supplier-provided mean often deviates from the true value and can thus adversely impact the derived scattering coefficient and scattering phase function. Uncertainties in the derived scattering coefficient and scattering phase function can also be introduced by the polystyrene refractive index, which varies quite significantly by

#387619 https://doi.org/10.1364/BOE.387619
Journal © 2020 Received 7 Jan 2020; revised 20 Feb 2020; accepted 24 Feb 2020; published 11 Mar 2020

Biomedical Optics EXPRESS

more than 0.5% in the literature [6,7]. Finally, the accuracy of the derived scattering coefficient can also be affected by the number density of the microspheres in the SPMs. This information is commonly given by suppliers as the solid content of suspension, from which the number density can be calculated.

The main challenge in accurate utilization of the Mie theory for derivation of optical properties is thus accurate characterization of the SPMs. While methods such as scanning and transmission electron microscopy offer characterization in terms of size, refractive index and solid content have to be determined separately. For size distribution one can also utilize dynamic light scattering. Extensive work has been done in the characterization of aerosol particles, where size and refractive index are the main unknowns [8–11]. However, the techniques are not directly applicable to the field of SPMs (the suspensions have to be atomized or nebulized) and equipment is not readily available in laboratories that work in the field of biomedical optics. Similar drawback can be inferred from advanced methods that include single particle trapping and characterization in terms of size and refractive index [12–14]. A simpler and more direct method for determination of the refractive index that is independent of the size and shape of the particles is the immersion liquid technique (ILT) [15,16]. This technique is based on transmittance measurement of particles suspended in media with different refractive indices. By observing the maximum of the transmission, the refractive index can be deduced. Finally, Ma *et al*. measured the complex refractive index of the SPM with a double-integrating sphere setup by observing diffuse reflectance and transmittance [7]. In this case the size and the number density of the SPMs had to be known *a priori*. A double integrating sphere was also recently utilized by Postelmans *et al*. for size distribution determination of SPMs [17]. However, in this case the refractive index of the polystyrene microspheres had to be set to bulk polystyrene [18].

The existing methods mostly provide either incomplete or complicated solutions to the problem of SPM characterization. In this regard, multiple methods would have to be utilized to separately yield the size, solid content and refractive index of polystyrene microspheres. Not only that some methods require demanding experimental equipment, using multiple methods to characterize SPMs is time and sample consuming.

In this study, we present in detail a simple ILT-inspired method for characterization of SPMs that can be deployed in virtually every laboratory or institution since it requires only a collimated transmission setup. Our method is based on transmittance measurements of SPMs immersed in an aqueous sucrose solution with different mass concentrations of sucrose (also known as Brix values), where the reference measurement at each Brix value is the equivalent transparent aqueous sucrose solution. From there, the scattering coefficient is obtained through the Beer-Lambert law and fitted using the Mie theory derived scattering coefficient. Since our proposed method relies on the properties of aqueous solution of sucrose, we first provide the refractive index and density as a function of Brix. Secondly, we show the sensitivity of the scattering coefficient on the refractive index and size of the polystyrene microspheres. Thirdly, we discuss in detail the validity of the Beer-Lambert law which can be simply used to yield the scattering coefficient. Finally, we test the proposed method on several commercially available SPMs.

2. Materials and methods

2.1. Mie theory and derived quantities

Polystyrene microspheres obtained from various suppliers are usually not entirely monodisperse and thus the derived quantities used in this study depend on the size distribution function $n(d)$, which is usually given by a Gaussian model

$$n(d) = Ce^{-\frac{(d-\bar{d})^2}{2\sigma^2}}, \tag{1}$$

Biomedical Optics EXPRESS

where $\bar{d}$ represents the mean diameter of the polystyrene microspheres, σ the standard deviation of the size distribution and C is the normalization constant defined as

$$\int_{-5\sigma+\bar{d}}^{5\sigma+\bar{d}} n(d)\mathrm{d}d = \frac{N}{V} = \tilde{n}\ , \tag{2}$$

where N represents the total number of microspheres in a SPM volume V resulting in number density $\tilde{n}$. The above integration limits are deliberately set to $\pm 5\sigma$, where the Gaussian distribution falls approximately to 0. For the values of $\bar{d}$ and σ used in our manuscript, such definition avoids physically meaningless negative diameters and high diameters at which the available numerical implementation of the Mie theory becomes inaccurate [5,19]. Note that we can also define dimensionless probability distribution function from Eq. (2), $p(d) = n(d)/\tilde{n}$, with a unity integral. Suppliers usually provide the number density $\tilde{n}$ of the microspheres as solid content s_c, which is defined as the ratio between the mass of the microspheres and the total volume of the sample SPM. The relationship between the number density $\tilde{n}$ and solid content s_c is given as

$$\tilde{n} = \frac{s_c}{\bar{V}_{\mathrm{one}}\ \rho_{\mathrm{poly}}}\ , \tag{3}$$

where ρ_{poly} is the density of the polystyrene (1.05 g/ml) and $\bar{V}_{\mathrm{one}}$ the average volume of one polystyrene microsphere defined as

$$\bar{V}_{\mathrm{one}} = \int_{-5\sigma+\bar{d}}^{5\sigma+\bar{d}} \frac{\pi d^3}{6} p(d)\ \mathrm{d}d\ . \tag{4}$$

The main derived quantity that will be used in our study is the scattering coefficient

$$\mu_s(\lambda) = \tilde{n} \int_{-5\sigma+\bar{d}}^{5\sigma+\bar{d}} p(d)\ \sigma_{\mathrm{sc}}\left(\frac{\pi d n_{\mathrm{m}}(\lambda)}{\lambda}, \frac{n_{\mathrm{s}}(\lambda)}{n_{\mathrm{m}}(\lambda)}\right)\mathrm{d}d\ , \tag{5}$$

where λ is the wavelength of light in vacuum, σ_{sc} the scattering cross section given as a function of the dimensionless size parameter and relative refractive index. The wavelength dependent parameters n_{s} and n_{m} stand for the refractive indices of polystyrene microspheres and medium. The scattering cross section σ_{sc} for spherical scatterers can be obtained from Mie theory with numerical approaches readily available in the book by Bohren and Huffman [5] and implemented by Mätzler [19]. Figure 1(a) shows a few examples of the wavelength-dependent scattering coefficients for various diameters $\bar{d}$ of polystyrene microspheres suspended in water with σ set to 3% of the nominal $\bar{d}$, $n_{\mathrm{s}}(\lambda)$ taken from [6] and $n_{\mathrm{m}}(\lambda)$ from [20].

2.2. Transmittance and scattering coefficient measurement

Transmittance measurements were performed using 10 mm path length glass cuvettes (OS 100-10-20, Hellma Analytics, Hellma GmbH & Co. KG, Müllheim, Germany) and a cuvette holder (CUV-UV/VIS, Avantes, Apeldoorn, The Netherlands). Light from a broadband tungsten-halogen light source (SLS201/M, Thorlabs Inc., New Jersey, USA) was delivered to the cuvette holder using a 200 µm optical fiber, where it was collimated by a lens ($f = 8.7$ mm CUV-UV/VIS, Avantes). A second lens ($f = 8.7$ mm) was used to collect the light, which was then transmitted to a spectrograph-based spectrometer (ImSpector V10E 400-1000 nm, Specim, Spectral Imaging Ltd., Oulu, Finland) by a second 200 µm optical fiber (Fig. 1(b)). The transmittance was defined as a ratio of the dark corrected signal obtained through the cuvette containing the SPM and the dark corrected signal through the same cuvette containing transparent aqueous sucrose solution with the same medium refractive index as the SPM. The wavelength range considered in our study spanned from 500 to 800 nm.

If a low number density SPM is investigated, the scattering coefficient μ_{s} can be obtained from transmittance through the Beer-Lambert law $\mu_s = -\ln T/d$, where T is the measured

Biomedical Optics EXPRESS

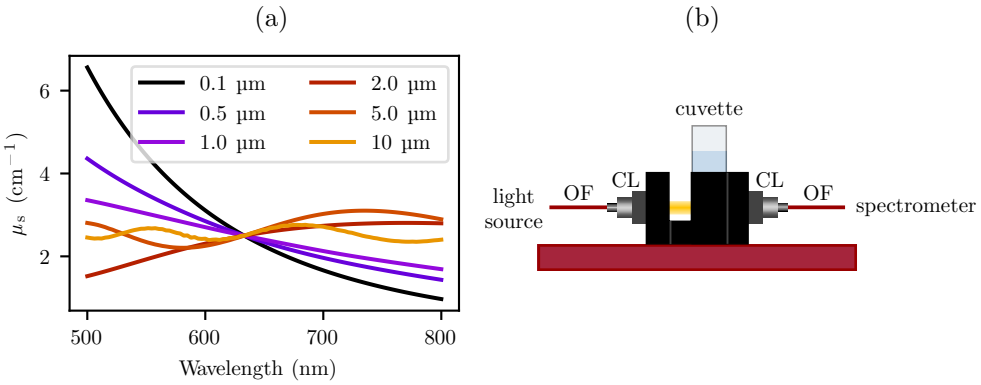

Fig. 1. (a) Wavelength-dependent scattering coefficient (μ_s) of SPMs calculated using Mie theory for several diameters given in the legend. All of the μ_s spectra are normalized to 2.5 cm^{-1} at 633 nm. (b) Transmittance measurement setup utilizing the cuvette holder CUV-UV/VIS with 200 µm optical fibers (OF) and two $f = 8.7$ mm collimating lens (CL).

transmittance and d is the cuvette path length. Since in general, the Beer-Lambert law returns the attenuation coefficient, the validity of the attenuation coefficient being equal to the scattering coefficient is discussed in the Section 3.3 using Monte Carlo simulations.

2.3. Parameter optimization procedure

Unknown parameters of the SPMs in our study involve the solid content s_c, refractive index $n_s(\lambda)$ and diameter d of the microspheres. The solid content usually changes after a long shelf time due to potential water evaporation. The refractive index $n_s(\lambda)$ and diameter d of the microspheres are usually provided only approximately by suppliers or in the literature.

We have modeled $n_s(\lambda)$ as a one-term Sellmeier equation (λ specified in meters)

$$n_s(\lambda) = \sqrt{1 + \frac{a}{1 - 10^{-14}\, b\, \lambda^{-2}}}\,. \tag{6}$$

While the standard deviation of the size distribution of polystyrene microspheres can be included as an unknown parameter, we have found that the influence of the distribution on the scattering coefficient is much less pronounced than the influence of other parameters and was thus set to a constant value usually provided by the supplier.

In total, we are faced with a problem of optimizing 4 unknown parameters (s_c, d, a, b) by fitting the Mie theory predicted scattering coefficient to measurements. While spectral regularization over a wavelength range from 500 to 800 nm yields many measurement points, we show in Section 3.4 there is a significant crosstalk between the unknown parameters, if only a single SPM is used. We have found that this crosstalk can be alleviated, if the starting SPM is diluted in aqueous sucrose solutions with different Brix values thus changing the refractive index of the surrounding medium n_m. Therefore, the proposed cost function that is optimized can be written as

$$CF(s_c,\ d,\ a,\ b) = \sum\nolimits_{B_i} \sum\nolimits_{\lambda_j} [\hat{\mu}_s(B_i, \lambda_j) - \mu_s(s_c,\ d,\ n_m(B_i, \lambda_j), n_s(a,\ b,\ \lambda_j), \lambda_j)]^2, \tag{7}$$

where $\hat{\mu}_s$ represents the measured scattering coefficient, which depends on the wavelength λ_j and Brix value B_i of i-th SPM diluted by an aqueous sucrose solution. The Mie theory predicted scattering coefficient μ_s (as defined in Eq. (5)) depends on the solid content s_c, diameter d and refractive index of the medium n_m and polystyrene n_s. The medium refractive index further depends on Brix B_i and wavelength λ_j, while polystyrene refractive index depends on parameters a and b of the Sellmeier equation, and wavelength λ_j.

Biomedical Optics EXPRESS

Our procedure involves the optimization of parameters (s_c, d, a, b) using 31 wavelength points uniformly distributed between 500 and 800 nm and five different SPMs with medium Brix values of 0.0, 20.0, 30.0, 50.0 and 60.0%. Optimization was performed using Trust Region Reflective algorithm with lower boundaries set to (a = 1.0, b = 1.0 m^2, d = 0.1 μm, s_c = 0.0 g/ml) and upper boundaries to (a = 4.0, b = 4.0 m^2, d = 2.0 μm, s_c = 1.0 g/ml). In Sect. 3.4, 16 initial values sets were utilized which were varied ± 30% from their nominal true values. In Sect. 3.5, a single set of initial values was used (a = 2.0, b = 3.0 m^2, d = 0.1 μm, s_c = 0.01 g/ml).

2.4. Sample preparation for transmittance measurements

As pointed out in the previous section, our optimization procedure utilizes five different dilutions of original SPMs with aqueous sucrose solution yielding different medium Brix values. In this way, the medium refractive index is varied to regularize the optimization. Since the transmittance of each resulting SPM is measured against a transparent reference with the same Brix value (to match the refractive index), each SPM requires a matching transparent aqueous sucrose solution without the scatterers.

For this study, we have diluted the original SPMs by knowing the approximate solid content, diameter and polystyrene refractive index beforehand. This prior knowledge was used to obtain scattering coefficients of final suspensions that are within the validity of the Beer-Lambert law (i.e., in the order of 1-4 cm^{-1}), which we discuss in Section 3.3. Although at least some approximate prior information is often available for SPMs from the suppliers, we later also describe a mixing procedure, when the specifications of the SPM are unknown.

Firstly, we prepared transparent solutions without the scatterers by mixing a specified quantity of deionized water and sucrose (BioXtra ≥99.5%, S7903-1KG, Sigma-Aldrich Inc.) to yield the target Brix value for five solutions given in Table 1, along with the required masses of water (m_{H2O}) and sucrose ($m_{sucrose}$). A vital step in the sample preparation is thorough mixing that results in optically uniform samples. Mixing proved to be particularly important and somewhat challenging for the samples with high Brix values, since the density and viscosity of the liquid increases significantly. These samples were mixed with a magnetic stirrer (ARE Heating Magnetic Stirrer, VELP Scientifica, Usmate, Italy) for roughly 10 minutes and sonicated in an ultrasonic bath (Ultra 8020, James Products Europe Limited, England) to eliminate any bubbles that formed during the mixing step.

Table 1. The required amounts of deionized water (m_{H2O}) and sucrose ($m_{sucrose}$) to yield the target Brix value for a transparent solution.

Sample #	*Brix* (%)	m_{H2O} (g)	$m_{sucrose}$ (g)
1	0.00	10.0	0.00
2	20.0	40.0	10.0
3	30.0	23.3	10.0
4	50.0	10.0	10.0
5	60.0	6.67	10.0

Secondly, we prepared diluted SPMs in a two-step procedure to conserve with the amount of sucrose and to yield a smaller quantity of the final sample for easier mixing. In the first step, a pre-calculated volume of the original SPM (V_{orig}) was added to the volume of pure deionized water (V_{addH2O}). After thorough mixing with a magnetic stirrer, the second step involved extraction of a smaller volume of the diluted SPM (V_{ext}) to which we added the same amount of sucrose ($m_{sucrose}$) as in the corresponding transparent reference solutions, to obtain the same medium refractive index. The volumes are provided in Table 2 for all microsphere sizes that were tested experimentally in this study (obtained from microParticles GmbH, Berlin,

Biomedical Optics EXPRESS

Germany). Note that the preparation of sucrose-free sample 1 follows a simplified procedure that does not require addition of sucrose in the second step.

Table 2. Volumes of the original SPM (V_{orig}), added deionized water (V_{addH2O}) and extracted volume (V_{ext}) required to obtain five different samples of SPMs for three different sizes of microspheres. Note that 10.0 mg of sucrose was added to V_{ext} of samples 2-5.

		$d = 0.721$ µm, $s_c = 0.05$ g/ml		$d = 1.05$ µm, $s_c = 0.05$ g/ml		$d = 0.425$ µm, $s_c = 0.05$ g/ml	
Sample #	V_{orig} (ml)	V_{addH2O} (ml)	V_{ext} (ml)	V_{addH2O} (ml)	V_{ext} (ml)	V_{addH2O} (ml)	V_{ext} (ml)
1	0.3	189.8	0	231.8	0	111.0	0
2	0.4	161.0	40.12	206.9	40.12	91.78	40.12
3	0.4	123.1	23.40	162.2	23.40	69.28	23.41
4	0.4	62.26	10.03	86.20	10.03	34.14	10.03
5	0.4	39.16	6.689	55.55	6.688	21.18	6.692

Often the specifications, e.g. solid content s_c, of SPMs are unknown, especially after a long shelf time or after unrecorded dilutions. In this case, prior knowledge cannot be used to calculate the required volumes and masses of the original SPM, deionized water and sucrose. However, the following procedure can be used to yield the final scattering coefficient that is still within the validity of the Beer-Lambert law and introduces practically negligible errors in terms of mixtures.

Firstly, a small but easily measureable mass of original SPM is extracted and mixed with a required mass of sucrose to yield the target Brix value. The required mass of sucrose is calculated by using the total mass of the original SPM and disregarding the volume occupied by the scatterers. Note that in this case we make a crude approximation that sucrose can dissolve in the whole volume of the original SPM. Since for high solid contents the available aqueous volume is significantly smaller, we actually obtain a larger Brix value. Next, we separately mix a transparent aqueous sucrose solution with the true target Brix value. Subsequently, we add the solution to the SPM until the transmittance corresponds to the target scattering coefficient, where the Beer-Lambert law holds (i.e., in the order of 1-4 cm^{-1}). As a reference in the transmittance measurements, we use the transparent aqueous solution of sucrose. Finally, all the masses and dilutions should be monitored and recorded so that they can be traced back to the original SPM. The above procedure should be repeated for five target Brix values as given in Table 1.

While the above procedure initiates with a wrong Brix value in the SPM, it should be noted that upon dilution with the transparent aqueous sucrose solution with the correct Brix value, the final Brix value virtually coincides with the correct Brix value. This is a reasonable assumption since the final solid content of the diluted SPM is so small that can be neglected without introducing significant errors. For example, when the solid content of the original SPM is large, the error of the initial Brix value is also large. However, since the solid content is large, the SPM will have to be significantly diluted by the transparent equivalent, which will finally yield a suspension with a Brix value that is virtually the same as that of the transparent aqueous sucrose solution. Likewise, if the solid content of the original SPM is small, then the error of the initial Brix value is also small. By addition of the transparent equivalent, the error of the Brix value is further reduced.

Since possible errors of the Brix value directly translate to the errors of medium refractive index, we have evaluated the errors in terms of different solid contents (between 0.001 and 0.1 g/ml) of the original SPM and different target Brix values (between 0.0 and 60.0%). Figure 2 shows the maximum relative error of the medium refractive index n_{med} calculated across different solid contents and displayed as a function of the Brix value. It can be seen that the relative error of the medium refractive index never exceeds 0.05% and significantly decreases with increasing diameter of the microspheres. For 0.0% Brix value the error is 0%, since dilution is done with deionized water and the medium refractive index does not change from the initial one.

Biomedical Optics EXPRESS

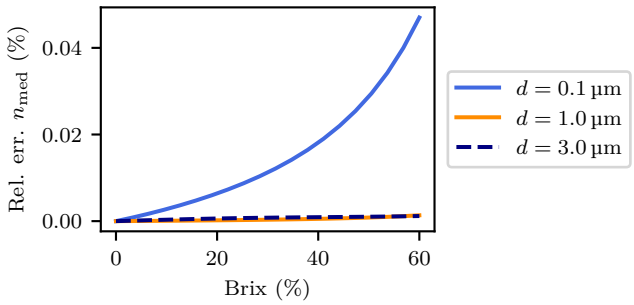

Fig. 2. Maximum relative error of the medium refractive index (n_{med}) of the final SPM calculated across different solid contents of the original SPMs given as a function of the target Brix values. The relative errors were evaluated for three different diameters given in legend.

Once the scattering coefficients of five polystyrene suspensions with different Brix values are measured, they can be fitted using Eq. (7) by optimizing the parameters of the original SPM, where the solid content s_c can be traced back through the recorded masses and dilutions of each suspension (i.e., all of the final SPMs share the same original SPM).

2.5. Refractive index and density of aqueous sucrose solution

The refractive index of aqueous sucrose solution is given in the literature mainly at the wavelength of 589.3 nm. Since the proposed method requires the medium refractive index at multiple wavelengths, we have utilized a commercial refractometer (Abbemat MW, Anton Paar GmbH, Graz, Austria) with which we were able to measure the refractive index at eight wavelengths including 436.3, 480.3, 514.2, 533.1, 546.1 589.3, 633.7 and 657.2 nm and at two temperatures, namely 20.0 and 25.0°C.

The density of the sucrose solution was measured at 25°C using a 50 ml certified pycnometer (ISOLAB Laborgeräte GmbH, Eschau, Germany).

2.6. Monte Carlo simulations

To investigate the effects of multiple scattering and anisotropy factor on the validity of the Beer-Lambert law, we have modeled light propagation through a glass cuvette with a custom-developed OpenCL implementation of the Monte Carlo method. The measurement setting was modeled as a multi-layer structure with source-cuvette and cuvette-detector distance set to 10 mm, cuvette wall thickness to 1.25 mm and cuvette path length to 10 mm. The refractive index of the medium surrounding the cuvette was set to 1.0, the refractive index of the cuvette was modeled as that of quartz [21] and the refractive index of the interior was modeled according to the Brix value of the sucrose solution. The source beam and the detector diameter were set to 4.0 mm with a beam divergence and detection acceptance angle of 0.66 degrees. Transmittance was defined as a ratio between the number of detected photon packets obtained through a glass cuvette filled with the SPM and with the reference transparent aqueous sucrose solution. For each simulation we have propagated 500 million photon packets. The simulations were performed on a personal computer (i7, 32 GB RAM, Nvidia GTX 1070).

Biomedical Optics EXPRESS

3. Results and discussion

3.1. Refractive index and density of aqueous sucrose solution

The refractive index and density of aqueous sucrose solution had to be measured to ensure accurate calculations of the scattering coefficient and solid content of the SPMs given a certain Brix value.

Tables 3 and 4 show the refractive index of the aqueous sucrose solution at two temperatures 20.0 and 25.0°C, and multiple wavelengths. The corresponding graphs of the aqueous sucrose solution refractive index as a function of wavelength and Brix value are presented in Fig. 3(a). While the refractive index was measured in the narrow range from 436.4 to 657.2 nm, it can be extrapolated up to 850 nm using a fitted three term Sellmeier equation without introducing significant errors. Extrapolation was tested on the refractive index of water measured by Daimon *et al*. [20], by fitting the three term Sellmeier equation to 8 wavelength points between 436.4 and 657.2 nm. Subsequently, the relative error between the true measured and fitted values was calculated in the range from 450 to 850 nm. The maximum error due to the extrapolation was located at 850 nm and amounted to merely 0.002% or at the 5th decimal place in the refractive index. Since we expect that the aqueous suspension of sucrose exhibits similar wavelength dependence of the refractive index, the extrapolation should not pose a problem.

Table 5 and Fig. 3(b) show the dependence of aqueous sucrose solution density on the Brix value. The density was measured at 7 points (red circles), to which a third order polynomial was fitted (shown with navy blue line in Fig. 3(b)).

Table 3. Wavelength dependent refractive index of aqueous sucrose solution measured at T = 20.0 °C.

Brix (%)	0.00	10.13	20.11	29.92	40.01	49.99	59.96
436.4 nm	1.34017	1.35554	1.37180	1.38911	1.40832	1.42894	1.45176
480.3 nm	1.33746	1.35273	1.36889	1.38608	1.40517	1.42566	1.44831
514.2 nm	1.33581	1.35098	1.36708	1.38423	1.40325	1.42365	1.44622
533.1 nm	1.33488	1.35005	1.36614	1.38325	1.40225	1.42263	1.44517
546.1 nm	1.33445	1.34954	1.36562	1.38272	1.40170	1.42204	1.44452
589.3 nm	1.33298	1.34803	1.36405	1.38111	1.40001	1.42030	1.44270
633.7 nm	1.33172	1.34675	1.36272	1.37973	1.39858	1.41881	1.44116
657.2 nm	1.33117	1.34619	1.36214	1.37914	1.39796	1.41818	1.44050

Table 4. Wavelength dependent refractive index of aqueous sucrose solution measured at T = 25.0 °C.

Brix (%)	0.00	10.13	20.11	29.92	40.01	49.99	59.96
436.4 nm	1.33967	1.35493	1.37118	1.38839	1.40756	1.42806	1.45084
480.3 nm	1.33696	1.35212	1.36827	1.38535	1.40442	1.42478	1.44740
514.2 nm	1.33531	1.35038	1.36646	1.38349	1.40251	1.42277	1.44532
533.1 nm	1.33439	1.34951	1.36552	1.38253	1.40151	1.42176	1.44428
546.1 nm	1.33395	1.34901	1.36502	1.38200	1.40097	1.42117	1.44365
589.3 nm	1.33250	1.34751	1.36347	1.38038	1.39928	1.41943	1.44184
633.7 nm	1.33123	1.34621	1.36213	1.37900	1.39785	1.41795	1.44030
657.2 nm	1.33069	1.34566	1.36158	1.37842	1.39723	1.41731	1.43969

Biomedical Optics EXPRESS

Table 5. Density of aqueous sucrose solution as a function of Brix value measured at 25°C.

Brix (%)	Density (g/cm^3)
0.00	0. 9962
0.10	1.0365
0.20	1.0794
0.30	1.1244
0.40	1.1742
0.50	1.2268
0.60	1.2845

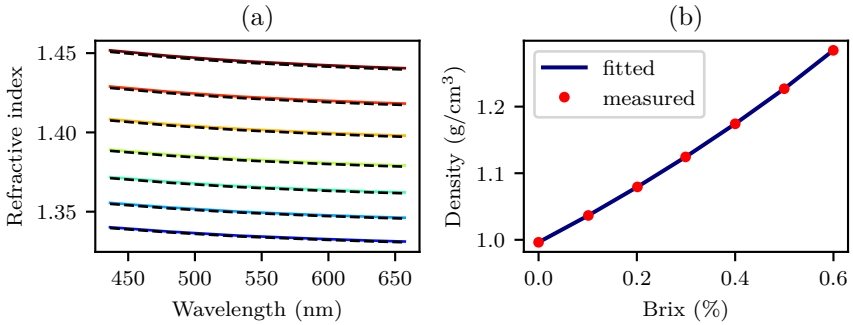

Fig. 3. (a) Refractive index of the aqueous sucrose solution as a function of wavelength and Brix value (colors from blue to red correspond to increasing Brix values) given at two temperatures 20°C (solid lines) and 25°C (nearly overlapping black dashed lines). (b) Density of the aqueous sucrose solution as a function of Brix value.

3.2. *Influence of the polystyrene refractive index and diameter deviations on the Mie theory derived reduced scattering coefficient*

One of the main optical properties of turbid phantoms is the reduced scattering coefficient μ_s'. Advantage of the SPM-based optical phantoms over other alternatives is that the optical properties such as the reduced scattering coefficient can be derived using Mie theory. However, the calculated quantities significantly depend on the optical and physical properties provided for the SPM. Since the polystyrene refractive index given within the literature can vary by more than 0.5%, it is important to study these dependencies. Figure 4(a) depicts the literature provided polystyrene refractive indices and the red region demonstrates the relative deviation between two commonly cited values. Although the relative difference of 0.5% might seem insignificant, such discrepancies in the polystyrene refractive index result in much higher relative differences of more than 5% in the derived reduced scattering coefficient for 1-µm-sized spheres (Fig. 4(b)). In other words, the relative error that propagates from the polystyrene refractive index to the reduced scattering coefficient is amplified approximately by a factor of 10. For example, the blue region in Fig. 4(a) corresponds to ± 0.2% relative deviation of the polystyrene refractive index and results in ± 2% relative deviation in the derived reduced scattering coefficient for 1 µm sized spheres.

Diameter uncertainty is much less amplified than the uncertainty of the refractive index. Figure 5 shows the reduced scattering coefficient for 1 µm SPM with the blue region representing the ± 2% relative deviation in the nominal diameter. It can be seen that the relative deviation

Biomedical Optics EXPRESS

in the reduced scattering coefficient is also approximately 2% (red region), so the errors are propagated without amplification.

Based on these results, the relative error of the refractive index affects the reduced scattering coefficient much more than the diameter. Therefore, we aim to determine the refractive index within ± 0.2% of the reference value, while the diameter roughly within ± 2% of the reference diameter.

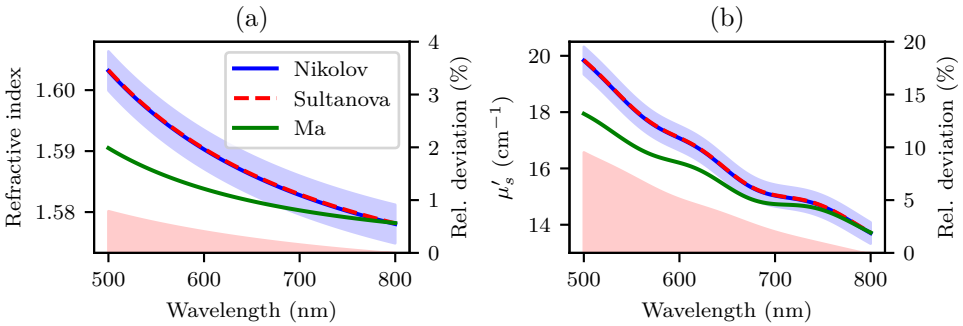

Fig. 4. (a) Refractive index of polystyrene microspheres as given by different authors (Nikolov *et al.* [6], Sultanova *et al.* [18] and Ma *et al.* [7]). Red region represents the relative deviation between the refractive indices as reported by Nikolov *et al.* and Ma *et al.* Blue region represents the ± 0.2% variation in the refractive index of Nikolov *et al.* (b) Reduced scattering coefficient (μ_s') for 1 μm polystyrene microspheres in a water suspension as given by Mie theory using the polystyrene refractive index from the listed sources. Red region denotes the relative deviation between the reduced scattering coefficients calculated by the polystyrene refractive index from Nikolov *et al.* and Ma *et al.* Blue region represents the variation of reduced scattering coefficient as a consequence of the 0.2% variation in the polystyrene refractive index.

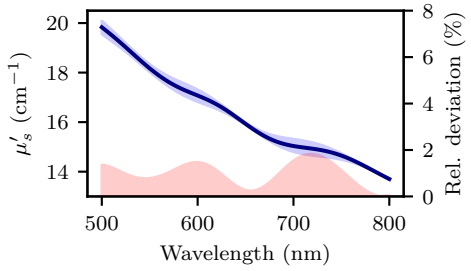

Fig. 5. Reduced scattering coefficient (μ_s') for 1 μm polystyrene microspheres in a water suspension as given by the Mie theory. Blue region represents the effect of ± 2% relative deviation of the diameter on the reduced scattering coefficient (red region shows the equivalent relative error).

Biomedical Optics EXPRESS

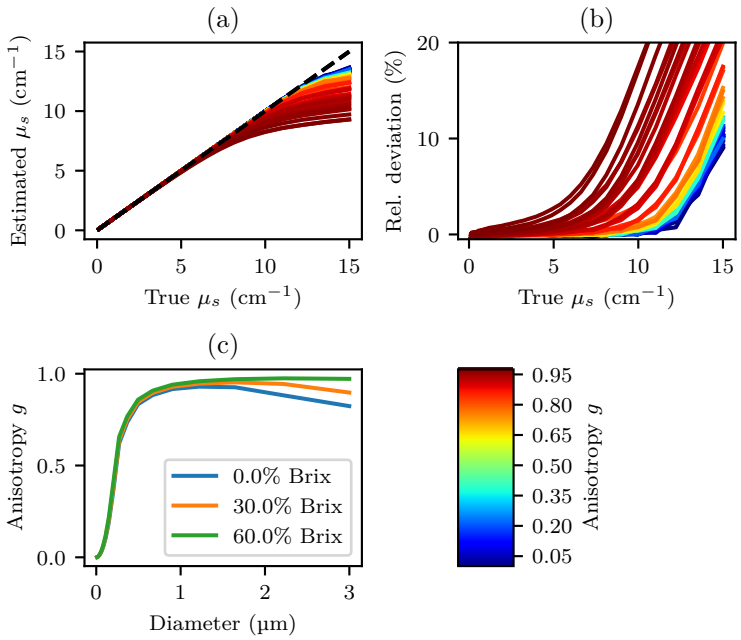

Fig. 6. (a) Relationship between the true input scattering coefficient (μ_s) and the scattering coefficient (μ_s) estimated by the Beer-Lambert law from Monte Carlo simulated transmittance. The lines are color coded to represent different anisotropy factors arising from different polystyrene microsphere diameters and Brix values used in the Monte Carlo simulations of transmittance (see the colorbar). (b) Relative deviation of the estimated scattering coefficient (μ_s) from the true one as given in example (a). (c) Dependence of the anisotropy factor on the microsphere diameter and Brix values of the solution. All examples were calculated at a wavelength of 600 nm.

3.3. *Validity of the Beer-Lambert law*

The Beer-Lambert law relates the transmittance to the attenuation coefficient, which in non-absorbing purely scattering media is the scattering coefficient. However, the validity of the Beer-Lambert law can be broken by multiple scattering and high anisotropy factor of the scatterers. In the first case, the signal due to multiple scattering is not as highly attenuated as one would expect, since some of the light can be scattered back into the light path. In the second case, the anisotropy factor can hinder the validity due to increasing the amount of forward scattered light, which cannot be discriminated from unscattered light.

Figure 6(a) shows the relationship between the scattering coefficients (μ_s) estimated by the Beer-Lambert law from the Monte Carlo simulated transmittance and the true input scattering coefficient at a wavelength of 600 nm. Different colors represent different anisotropy factors as a result of polystyrene microsphere diameter variation from 0.01 to 3 μm submerged in an aqueous sucrose solution with Brix values varying from 0.0 to 60.0% (see the colorbar). We can clearly observe that the estimated scattering coefficient starts to deviate from the true scattering coefficients at high values. This difference is also more pronounced for high anisotropy factors. Both observations agree with the fact that at high scattering coefficients multiple scattering events start contributing to the transmittance signal and for high anisotropy factors more intense forward scattering is contributing to the transmittance signal. The absolute value of the relative deviation of the estimated scattering coefficient from the true scattering coefficient is presented in Fig. 6(b).

Biomedical Optics EXPRESS

We can observe that the relative deviation is less than 2% for true input scattering coefficient under 4 cm^{-1}.

Consequently, a scattering coefficient of approximately 2.5 cm^{-1} at 633 nm was enforced in our experiments, which ensured that the scattering coefficient across the utilized spectrum from 500 to 800 nm would not significantly exceed 4 cm^{-1}. In the experimental setting the target transmittance for a 10 mm cuvette would therefore lie around 8.2%. It should be noted that while using small scattering coefficients even below 1 cm^{-1} could prove useful in terms of Beer-Lambert law validity, the relative error that propagates into the scattering coefficient from the transmittance measurement increases significantly when transmittance approaches 100%, therefore the measured scattering coefficient should lie between 1 and 4 cm^{-1}.

In Fig. 6(c), which shows the dependence of the anisotropy factor on the sphere diameter for three different Brix values of the solution, we can see that the anisotropy rises with the sphere diameter and Brix value. However, as given in Fig. 6(b), the relative deviation of the estimated scattering coefficient does not exceed 2% for sphere diameters up to 3 μm and for true input scattering coefficients under 4 cm^{-1}.

3.4. Scattering coefficient fitting ambiguity

The most straightforward approach in the optimization of four unknown parameters (s_c, d, a and b) would be to fit the Mie theory predicted scattering coefficient to a single measured spectrum $\mu_s(\lambda)$, i.e. choosing only one term in the sum over B_i, Eq. (7). In this way, only a single dilution of the original SPM would be required. However, to show that several dilutions with different B_i values are required, we firstly investigated the uniqueness of the optimization process when using a single and five different B_i values by setting the initial values of optimized parameters to ± 30% from their true values. The optimization process was performed on the wavelength-dependent scattering coefficient $\mu_s(\lambda)$ obtained from the Monte Carlo simulated transmittance through a 10 mm cuvette containing 1-μm-sized SPM to circumvent potential errors that would be introduced by the measurements but still account for the characteristics of the experimental setup. Since 4 unknown parameters were optimized, 16 initial value sets were tested.

The relative deviation of the estimated s_c, d and n_s (based on the parameters a and b) from their respective true values is collected in Fig. 7 for the case of single and five different B_i values in the optimization process. It can be observed that when using only a single dilution (Fig. 7(a)), the optimized values for many initial values significantly differ from their respective true values. This would suggest that the optimization process gets trapped in a local minimum. In contrast, when using five different B_i values (Fig. 7(b)) the optimization process always ends in the global minimum, where the optimized values are virtually the same as the true ones. Although a single or five B_i dilutions are investigated in our study, we have found that three B_i dilutions are already adequate for reliably locating the global minimum.

Figure 8(a) outlines an example from the above optimization test that uses a single B_i dilution. The scattering coefficient seems to nicely fit although the optimized values ($s_c = 0.0325$ g/ml, $d = 0.661$ μm, $n_s = 1.714$) deviate significantly from the true values ($s_c = 0.05$ g/ml, $d = 1.00$ μm, $n_s = 1.587$). Using these optimized values to represent the scattering coefficient of five B_i dilutions, one can observe that only one of the five spectra is fitted well (Fig. 8(b)). Therefore, in the case of a single B_i dilution, the optimization process would stop, while in the case of five B_i dilutions, the optimization process would continue until all five scattering coefficients are fitted well and the estimated values do not deviate significantly from their respective true values.

The above results suggest that when using only a single B_i dilution in the optimization process, different estimated parameters can yield the same scattering coefficient. Therefore, the parameters experience significant crosstalk that is eliminated when using several B_i dilutions in the optimization process. To further demonstrate why a single B_i dilution would be insufficient to discriminate between s_c, d and n_s, Fig. 9(a) shows the effect of the diameter d and Fig. 9(b)

Biomedical Optics EXPRESS

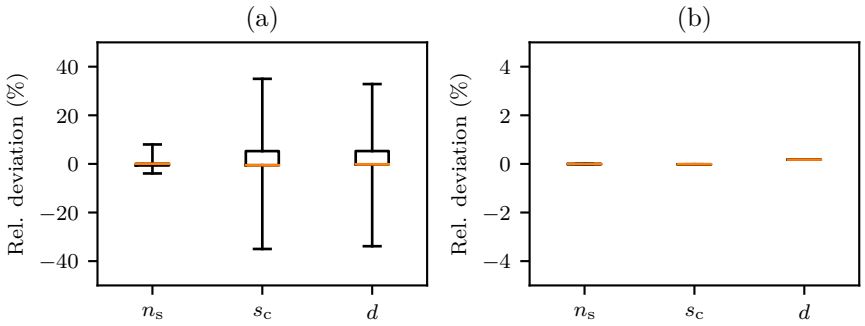

Fig. 7. Relative deviation of the estimated s_c, d and n_s (based on the parameters a and b) from their true counterparts when fitting the Mie theory predicted scattering coefficient to the scattering coefficient obtained from Monte Carlo simulated transmittance starting from 16 different initial value sets. (a) Results obtained for a single dilution and (b) for five dilutions with different B_i values.

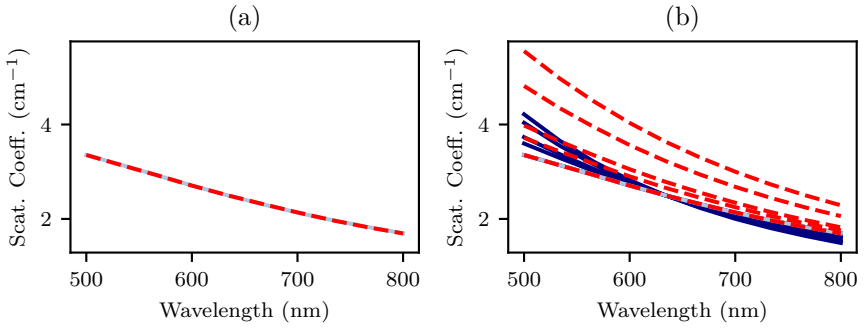

Fig. 8. (a) Fitted scattering coefficient (dashed red) and scattering coefficient obtained from Monte Carlo simulated transmittance for a single dilution of 1 µm SPM (light blue). (b) Scattering coefficients (dashed red) predicted by Mie theory for parameters (s_c, d, a and b) obtained from example (a) and scattering coefficients obtained from Monte Carlo simulated transmittance for five dilutions with different B_i values of 1 µm SPM (navy blue and a light blue line from example (a)).

Biomedical Optics EXPRESS

the effect of the polystyrene refractive index n_s on the scattering cross section of nominally 1 μm microspheres. The scattering coefficient is obtained by multiplying the scattering cross section and the number density of the scatterers which is directly connected to the solid content s_c (Eq. (3)). Therefore, changing the three parameters leads to multiplicative changes in the scattering coefficient and is thus difficult to discriminate when using only a single B_i dilution.

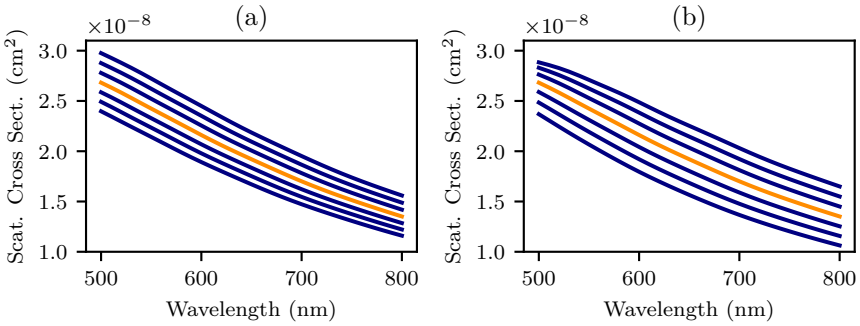

Fig. 9. (a) The effect of the diameter d on the scattering cross section of polystyrene microspheres. The diameter was varied by ± 4% from the nominal value of 1 μm using 7 uniformly spaced points. (b) The effect of the polystyrene refractive index n_s on the scattering cross section. The refractive index was varied by ± 2% from its nominal value [6] using 7 uniformly spaced points. The nominal scattering cross section in both cases is shown by the orange line.

3.5. Refractive index, size and solid content of SPMs

The proposed optimization method was tested on three different SPMs with mean sphere diameters equal to 0.425, 0.721 and 1.05 μm (further details in Table 5). To assess the repeatability of measurements, the 1.05 μm SPM was measured twice within 7 days.

Figure 10 shows the estimated polystyrene refractive index as a function of wavelength according to the optimized values of parameters a and b for different particles. Blue line represents the polystyrene refractive index as measured by Nikolov *et al*. [6] and the green region represents ± 0.2% relative deviation. It can be observed that for all sizes, the measured values of the polystyrene refractive index fall within the ± 0.2% region. Moreover, the refractive index of the 1.05 μm microspheres from the same SPM overlaps, which suggests good measurement repeatability. Although likely not the sole reason, the discrepancies between the three different SPMs could be due to batch-to-batch variations in the microspheres synthesis process as also suggested by Jones *et al*. [12]. The discrepancies could also be a consequence of the random uncertainties during the measurement procedure, which propagate into the transmittance and subsequently affect the scattering coefficients. To this end, however, further investigations showed that deliberate random perturbations of the scattering coefficients even up to 5% have not significantly changed the estimated refractive indices in Fig. 10.

The fitted scattering coefficients as modeled by the Mie theory (red dashed lines) and the measured scattering coefficients (navy blue) are presented in Fig. 11 for all the three test SPMs utilized in this study. One can observe that for all Brix dilutions (different lines within each graph) and microsphere sizes (a-d), the match is excellent. The red region represents the relative root-mean-square (RMS) error calculated between the fitted and measured scattering coefficients across the different Brix dilutions for each test case. For all except the last case (Fig. 11(d)), the relative RMS error is mainly below 1%, while for the 0.425 μm microspheres, the RMS error seems to be closer to 2%. It should be noted that the measured scattering coefficients do not

Biomedical Optics EXPRESS

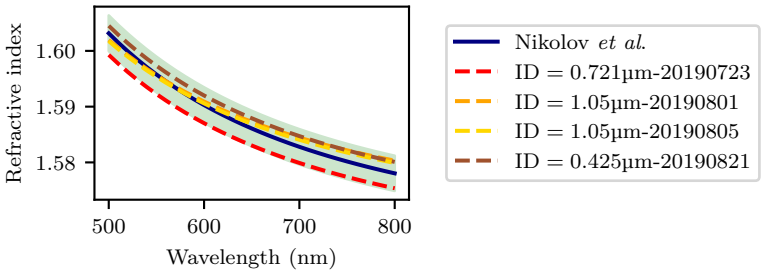

Fig. 10. Estimated refractive index as a function of the wavelength for three different SPMs (0.425, 0.721 and 1.05 µm). The estimation for 1.05 µm microspheres was repeated twice. Green region represents ± 0.2% relative deviation from the polystyrene refractive index as measured by Nikolov *et al.* [6]

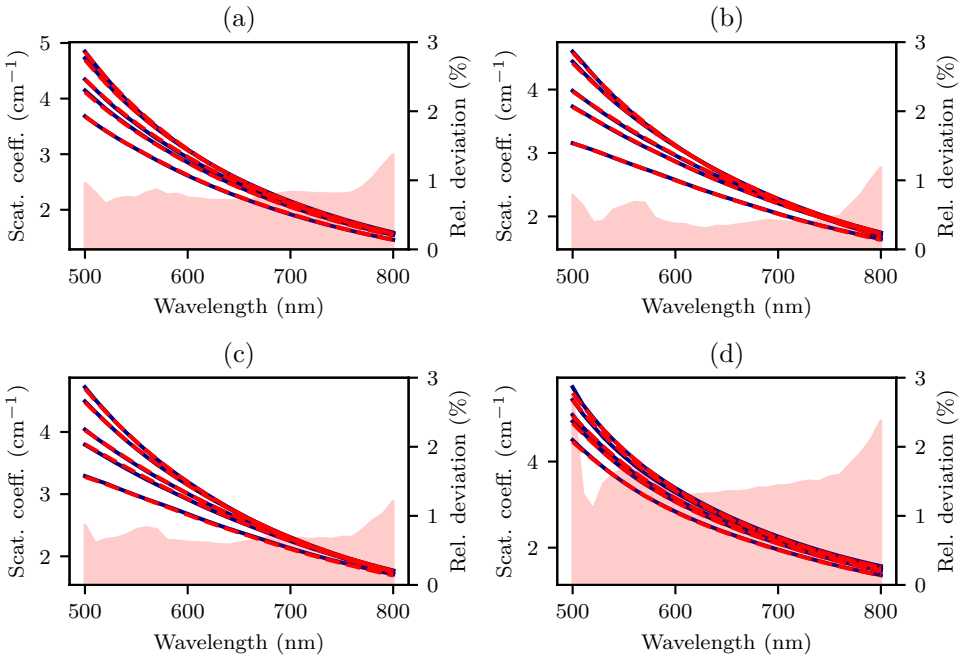

Fig. 11. Measured (navy blue) and fitted (dashed red) scattering coefficients of 0.721 µm (a), 1.05 µm (b) and (c), and 0.425 µm (d) using the proposed method. The red region represent the RMS error calculated between the fitted and measured scattering coefficients across the different Brix dilutions for each test case.

cross the target 2.5 cm^{-1} at 633 nm as set out in Section 3.3. This is because the SPM dilutions were made by assuming that the values of the solid content and diameter as specified by the supplier are completely true. Due to small differences in the two parameters and also due to errors during the mixing procedure, the final scattering coefficient slightly deviated from the target value. However, the masses of constituents were precisely recorded during the dilution and subsequently traced back to the original SPM.

Biomedical Optics EXPRESS

Finally, the estimated values of remaining parameters (s_c and d) are given in Table 6 along with the supplier data. In addition, we also determined the s_c by evaporating a sample of the original SPM and then measuring the mass of the residue. The relative deviation of the estimated parameters is given in parenthesis and is for s_c calculated from the measured mass of the residue, while for the diameter d from the supplier data. The relative deviation of the s_c never exceeds 2% and follows the reference values quite nicely. However, the diameter seems to deviate slightly more from the supplier-provided values.

Table 6. Solid content (s_c) and sphere diameter (d) of the polystyrene microsphere suspension as provided by the supplier (Supplier data), as calculated by our fitting method (Extracted) and as measured through the mass of the residue after sample evaporation (Mass).

	Supplier data		Extracted		Mass
Particle IDs	s_c (g/ml)	d (µm)	s_c (g/ml)	d (µm)	s_c (g/ml)
0.721µm-23072019	0.050	0.721 ± 0.02	0.05012 (0.80%)	0.7334 (1.72%)	0.04972
1.050µm-01082019	0.050	1.05 ± 0.03	0.05194 (1.51%)	1.0058 (–4.21%)	0.05117
1.050µm-05082019	0.050	1.05 ± 0.03	0.05232 (1.74%)	1.0070 (–4.09%)	0.05143
0.425µm-21082019	0.050	0.425 ± 0.01	0.04986 (–0.28%)	0.4353 (2.41%)	0.05000

In our experience, the supplier-provided diameter often deviates from the true value and we have come across this problem often when dealing with SPM-based optical phantoms. Especially, when the optical phantoms were used with optical fiber probes that included small source-detector separations [22,23], where the acquired reflectance spectrum exhibits oscillations that are due to the scattering phase function dependence on the wavelength. The signature of these oscillations also significantly depends on the diameter of the microspheres. In Fig. 12, we present reflectance spectra of 1.05 µm SPM as measured with an optical fiber probe with a source-detector separation of 220 µm. Additionally, we also show Monte Carlo simulated reflectance spectra using Mie theory derived scattering phase functions for four different diameters (1.007, 1.021, 1.05 and 1.07 µm) and with the polystyrene refractive index estimated by the proposed method. It can be seen that the reflectance spectra simulated for 1.007 and 1.021 µm SPMs seem to fit best the measured reflectance, with 1.021 µm being the optimal. Figure 12 indicates that the supplier-provided value of 1.05 µm might not be accurate and could just be an estimate provided as a result of the controlled manufacturing process. Furthermore, both the proposed method and the measured reflectance with an optical fiber probe suggest that the true diameter is significantly below 1.05 µm. Since the simulated reflectance of a 1.021 µm microsphere suspensions seems to best fit the measurements, the estimate of our method is off by only –1.4% and not by 4.2%, as would be inferred from the supplier-provided data in Table 6.

Biomedical Optics EXPRESS

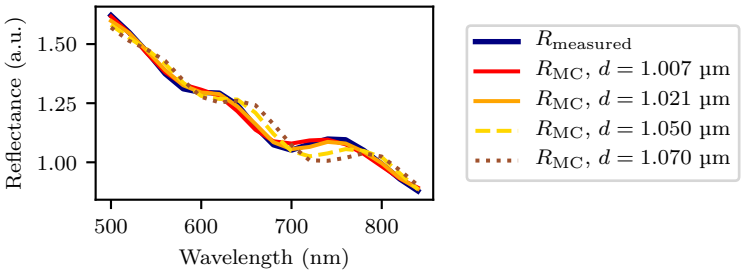

Fig. 12. Measured and modeled reflectance spectra (see legend) of SPM as acquired with an optical fiber probe at a 220 µm source-detector separation for different diameters of microspheres.

4. Conclusion

Characterization of SPMs in terms of refractive index, size and solid content is important for accurate calculation of optical properties of SPM-based turbid phantoms. For this purpose, we have proposed a simple method that is based on collimated transmittance measurements of SPMs diluted by different sucrose solutions. We have shown that such measurements allow simultaneous estimation of the refractive index, size and solid content. Thus, sucrose-based dilution is the key to accurate estimation and to the best of our knowledge, it has not been utilized before. With the proposed method we were able to obtain the refractive index within 0.2%, the microsphere size to approximately 15 nm and solid content within 2% of their respective reference values. The obtained values nicely fall within the requirements set out in the Section 3.2, where the refractive index should be known within 0.2% and size within 2% of their reference values to yield the scattering coefficient within 2%.

Further work on the proposed method includes characterization of the region of validity especially in terms of the size of the polystyrene microspheres. Up to this point, the proposed method was tested for microspheres between 0.425 and 1.05 µm, although according to the validity of the Beer-Lambert law, the method should work without any modifications for polystyrene microspheres up to 3.0 µm. Additionally, the proposed method should be investigated on monodisperse microspheres of other materials such as silica, which are also commonly used for scattering in turbid phantoms. Finally, we believe that the determination of refractive index, size and solid content could be further improved by incorporating additional information in terms of reflectance measured with optical fiber probes at small source-detector separations as was shown in Fig. 12.

Funding

Javna Agencija za Raziskovalno Dejavnost RS (J2-7211, J2-8173, P2-0232).

Disclosures

The authors declare no conflicts of interest.

References

1. X. U. Zhang, "Single fiber reflectance spectroscopy calibration," J. Biomed. Opt. **21**(10), 100502 (2016).
2. B. S. Nichols, N. Rajaram, and J. W. Tunnell, "Performance of a lookup table-based approach for measuring tissue optical properties with diffuse optical spectroscopy," J. Biomed. Opt. **17**(5), 057001 (2012).
3. L. Spinelli, M. Botwicz, N. Zolek, M. Kacprzak, D. Milej, P. Sawosz, A. Liebert, U. Weigel, T. Durduran, F. Foschum, A. Kienle, F. Baribeau, S. Leclair, J.-P. Bouchard, I. Noiseux, P. Gallant, O. Mermut, A. Farina, A.

Biomedical Optics EXPRESS

Pifferi, A. Torricelli, R. Cubeddu, H.-C. Ho, M. Mazurenka, H. Wabnitz, K. Klauenberg, O. Bodnar, C. Elster, M. Bénazech-Lavoué, Y. Bérubé-Lauzière, F. Lesage, D. Khoptyar, A. A. Subash, S. Andersson-Engels, P. Di Ninni, F. Martelli, and G. Zaccanti, "Determination of reference values for optical properties of liquid phantoms based on Intralipid and India ink," Biomed. Opt. Express **5**(7), 2037–2053 (2014).

4. S. K. V. Sekar, A. Pacheco, P. Martella, H. Li, P. Lanka, A. Pifferi, and S. Andersson-Engels, "Solid phantom recipe for diffuse optics in biophotonics applications: a step towards anatomically correct 3D tissue phantoms," Biomed. Opt. Express **10**(4), 2090–2100 (2019).
5. C. F. Bohren and D. R. Huffman, *Absorption and Scattering of Light by Small Particles* (John Wiley & Sons, 1983).
6. I. D. Nikolov and C. D. Ivanov, "Optical plastic refractive measurements in the visible and the near-infrared regions," Appl. Opt. **39**(13), 2067–2070 (2000).
7. X. Ma, J. Q. Lu, R. S. Brock, K. M. Jacobs, P. Yang, and X.-H. Hu, "Determination of complex refractive index of polystyrene microspheres from 370 to 1610 nm," Phys. Med. Biol. **48**(24), 4165–4172 (2003).
8. S. Vratolis, P. Fetfatzis, A. Argyrouli, A. Papayannis, D. Müller, I. Veselovskii, A. Bougiatioti, A. Nenes, E. Remoundaki, E. Diapouli, M. Manousakas, M. Mylonaki, and K. Eleftheriadis, "A new method to retrieve the real part of the equivalent refractive index of atmospheric aerosols," J. Aerosol Sci. **117**, 54–62 (2018).
9. T. Galpin, R. T. Chartier, N. Levergood, and M. E. Greenslade, "Refractive index retrievals for polystyrene latex spheres in the spectral range 220–420 nm," Aerosol Sci. Technol. **51**(10), 1158–1167 (2017).
10. R. E. H. Miles, S. Rudić, A. J. Orr-Ewing, and J. P. Reid, "Influence of Uncertainties in the Diameter and Refractive Index of Calibration Polystyrene Beads on the Retrieval of Aerosol Optical Properties Using Cavity Ring Down Spectroscopy," J. Phys. Chem. A **114**(26), 7077–7084 (2010).
11. T. Eidhammer, D. C. Montague, and T. Deshler, "Determination of index of refraction and size of supermicrometer particles from light scattering measurements at two angles," J. Geophys. Res. **113**(D16), D16206 (2008).
12. S. H. Jones, M. D. King, and A. D. Ward, "Determining the unique refractive index properties of solid polystyrene aerosol using broadband Mie scattering from optically trapped beads," Phys. Chem. Chem. Phys. **15**(47), 20735 (2013).
13. Y. Pang, H. Song, and W. Cheng, "Using optical trap to measure the refractive index of a single animal virus in culture fluid with high precision," Biomed. Opt. Express **7**(5), 1672–1689 (2016).
14. P. Chylek, V. Ramaswamy, A. Ashkin, and J. M. Dziedzic, "Simultaneous determination of refractive index and size of spherical dielectric particles from light scattering data," Appl. Opt. **22**(15), 2302–2307 (1983).
15. B. N. Khlebtsov, V. A. Khanadeev, and N. G. Khlebtsov, "Determination of the Size, Concentration, and Refractive Index of Silica Nanoparticles from Turbidity Spectra," Langmuir **24**(16), 8964–8970 (2008).
16. I. Niskanen, K. Hibino, and J. Räty, "Immersion liquid techniques in solid particle characterization: A review," Talanta **149**, 225–236 (2016).
17. A. Postelmans, B. Aernouts, and W. Saeys, "Estimation of Particle Size Distribution from Bulk Scattering Spectra: Validation on Monomodal Suspensions," Anal. Chem. **91**(15), 10040–10048 (2019).
18. N. Sultanova, S. Kasarova, and I. Nikolov, "Dispersion Properties of Optical Polymers," Acta Phys. Pol., A **116**(4), 585–587 (2009).
19. C. Mätzler, "MATLAB functions for Mie scattering and absorption, version 2," *IAP Res. Rep* 8, (2002).
20. M. Daimon and A. Masumura, "Measurement of the refractive index of distilled water from the near-infrared region to the ultraviolet region," Appl. Opt. **46**(18), 3811–3820 (2007).
21. I. H. Malitson, "Interspecimen Comparison of the Refractive Index of Fused Silica," J. Opt. Soc. Am. **55**(10), 1205–1209 (1965).
22. P. Naglič, F. Pernuš, B. Likar, and M. Bürmen, "Limitations of the commonly used simplified laterally uniform optical fiber probe-tissue interface in Monte Carlo simulations of diffuse reflectance," Biomed. Opt. Express **6**(10), 3973–3988 (2015).
23. P. Naglič, F. Pernuš, B. Likar, and M. Bürmen, "Estimation of optical properties by spatially resolved reflectance spectroscopy in the subdiffusive regime," J. Biomed. Opt. **21**(9), 095003 (2016).